



Robust drug bioavailability and safety for rheumatoid arthritis therapy using D-amino acids-based supramolecular hydrogels



Shaodan Ma^{a,b,1}, Shunan Gu^{c,1}, Jinwei Zhang^{c,1}, Weizhong Qi^c, Zhaowei Lin^c, Weicheng Zhai^a, Jie Zhan^d, Qi Li^{c,**}, Yanbin Cai^{a,***}, Yao Lu^{c,e,*}

^a Department of Cardiology, Laboratory of Heart Center, Zhujiang Hospital, Southern Medical University, Sino-Japanese Cooperation Platform for Translational Research in Heart Failure, Guangdong Provincial Biomedical Engineering Technology Research Center for Cardiovascular Diseases, Guangzhou, 510280, China

^b Shenshan Medical Center, Sun Yat-sen Memorial Hospital, Sun Yat-sen University, Shanwei, 516600, China

^c Department of Joint and Orthopedics, Orthopedic Center, Zhujiang Hospital, Southern Medical University, Guangzhou, 510280, China

^d Department of Laboratory Medicine, Guangdong Engineering and Technology Research Center for Rapid Diagnostic Biosensors, Nanfang Hospital, Southern Medical University, Guangzhou, 510515, China

^e Guangdong Key Lab of Orthopedic Technology and Implant, Guangzhou, 510010, China

ARTICLE INFO

Keywords:

Rheumatoid arthritis
Supramolecular hydrogel
D-amino acids
Methotrexate
Drug delivery system

ABSTRACT

Long-term use of disease-modifying anti-rheumatic drugs (DMARDs) such as methotrexate (MTX) shows clinical benefits for rheumatoid arthritis (RA) treatment. However, there are growing concerns over the adverse effects of systemic drug administration. Therefore, a strategy that can enhance drug bioavailability while minimizing side effects is urgently needed, but remains a challenge in RA therapy. To this end, here we conjugated MTX with a supramolecular self-assembling hydrogel composed of D-amino acids with a sequence of G^DF^DF^DY. It was shown that MTX-G^DF^DF^DY hydrogels exhibited a favorable drug selectivity behavior that they increased MTX toxicity toward RA synoviocytes, but reduce toxicity toward normal cells. Moreover, MTX-G^DF^DF^DY hydrogels not only effectively inhibited the proliferation and migration of RA synoviocytes, but also inhibited the polarization of proinflammatory M1 type macrophages to reduce inflammation. After intra-articularly injected the hydrogels into the joints of adjuvant induced arthritis (AIA) mice, we found that MTX-G^DF^DF^DY hydrogels significantly alleviated RA syndromes of joint swelling and fever compared to L-configuration MTX-GFFY hydrogels and free MTX. Furthermore, MTX-G^DF^DF^DY hydrogels successfully protected cartilage though inhibiting synovial invasion and inflammation without causing systematic side effects. Therefore, D-amino acids supramolecular hydrogels can serve as an efficient and safe drug delivery system, showing a promising potential to improve RA therapy.

1. Introduction

Rheumatoid arthritis (RA) is a symmetric chronic autoimmune disease. With disease progression, joint deformities and the related systemic symptoms lead to the loss of joint function, disability, and reduce life expectancy of RA patients [1,2]. At present, non-steroidal anti-inflammatory drugs (NSAIDs), glucocorticoids, disease-modifying anti-rheumatic drugs (DMARDs), and biological agents are the clinic routines of RA [3]. Although these drug treatments have a certain effect on slowing down the disease progression and ameliorating joint inflammation, concerns of long-term efficacy and side effects of systemic drug

administration are growing. For example, long-term use of NSAIDs (e.g., etoricoxib) and DMARDs (e.g., methotrexate, MTX) may increase the risk of gastrointestinal bleeding and cause liver function impairment, respectively [4]. Patients taking glucocorticoids and biological agents (such as IL-6 inhibitors, TNF- α inhibitors, etc.) face a high risk of infection [5]. Therefore, improving therapeutic effect of drugs while minimizing their adverse effects is a daunting challenge in RA treatment.

Delivering drugs via biomaterials provides an alternative strategy for RA treatment. To date, various drug delivery systems including liposomes [6,7], carbon nanotubes [8,9], noble metal nanoparticles [10,11], and so on have been developed to improve the safety and bioavailability

* Corresponding author. Department of Joint and Orthopedics, Orthopedic Center, Zhujiang Hospital, Southern Medical University, Guangzhou, 510280, China.

** Corresponding author.

*** Corresponding author.

E-mail addresses: qili565@foxmail.com (Q. Li), skyer1@smu.edu.cn (Y. Cai), oayul@smu.edu.cn (Y. Lu).

¹ These authors contributed equally to this work.

of drugs. Among them, injectable hydrogels have drawn considerable attentions in RA research because they have good drug loading capacity and can be directly injected into inflammatory joints [12,13]. In recent years, peptide-based supramolecular hydrogels are developed as a new kind of hydrogels. These hydrogels with injectable and self-assemble properties can form via π - π stacking interactions of the peptides with certain amino sequences [14]. Moreover, they exhibit good biocompatibility, responsiveness, and mouldability, favoring biomedical applications [15,16]. Further, supramolecular hydrogels can serve as an efficient drug delivery system due to its high internal water content in the cross-linking system, which protects drugs from internal damage and thus improves drug retention time [17]. Therefore, peptide-based supramolecular hydrogels have been widely studied in oncology, tissue engineering, ophthalmology, biological detection, and other fields [18–20]. Taking advantage of the good drug delivering capability and biocompatibility, supramolecular hydrogels may be able to overcome the drawbacks of current clinically used drugs in RA treatment. Therefore, we aimed to develop supramolecular hydrogels with enhanced therapeutic effects on inflammatory synoviocytes but reduced cytotoxicity toward normal cells for RA therapy.

Natural amino acids are L-configuration while D-configuration amino acids are artificial. Interestingly, L-configuration and D-configuration supramolecular hydrogels exhibit distinct biological characteristics even they composed of the same amino acid sequences [21]. Yang et al. have developed peptides-based hydrogels to deliver hydroxycamptothecin (HCPT). They show that D-configuration HCPT-loaded hydrogels have a long-term stability in a water-soluble environment and exhibit a better tumor inhibiting effect relative to L-configuration hydrogels [22]. Li et al. have constructed NSAIDs loaded D-configuration peptides and find that D-configuration sequence peptides can significantly increase the selectivity of NSAIDs drugs, and thus reduce side effects in vitro [23]. Moreover, self-assembling hydrogels constructed by D-configuration amino acids also present an enzyme-instructed behavior and can selectively kill cancer cells that overexpress alkaline phosphatases [24]. Hence, using D-configuration amino acids to prepare supramolecular hydrogels may improve the therapeutic effect and biosafety of drugs in RA.

In this study, we synthesized a series of supramolecular peptides by using natural L-amino acids and D-configuration amino acids. The resultant GFFY and G^DF^DF^DY peptides were further conjugated with MTX, a first-line drug for RA treatment [25], through the reaction between carboxyl groups in MTX and the deaminated glycine in peptides. The as-prepared peptides could self-assemble into injectable hydrogels via π - π stacking interactions (Scheme 1a). We found that D-configuration MTX-G^DF^DF^DY hydrogels were better than MTX-GFFY hydrogels in terms of stability, drug releasing, and biocompatibility. More importantly, MTX-G^DF^DF^DY hydrogels inhibited not only the proliferation, migration, and invasion of RA synoviocytes, but also the polarization of proinflammatory M1 type macrophages. Consequently, after intra-articular injection of MTX-G^DF^DF^DY hydrogels, clinical symptoms including joint swelling and fever were significantly relieved in adjuvant induced arthritis (AIA) mice. Moreover, MTX-G^DF^DF^DY hydrogels effectively inhibited synovial hyperplasia, leading to a successful protection of articular cartilage and joint structure (Scheme 1b).

2. Experimental section

2.1. Materials

Amino acids, 2-(naphthalene-2-yl) acetic acid, and O-(benzotriazole-1-yl)-N,N,N,N-tetramethyluronium hexafluorophosphate (HBTU) were purchased from Bidepharm (Shanghai, China). 1-Pyrenemethylamine hydrochloride and trifluoroacetic acid (TFA) were obtained from Energy Chemical (Beijing, China). 2-Cl-Trityl chloride resin was bought from Nankai Resin Co. Ltd (Tianjin, China). N,N-Diisopropylethylamine (DIEA) was purchased from J & K (Beijing, China). Glycine, phenylalanine, tyrosine, and methotrexate were bought from Bidepharm

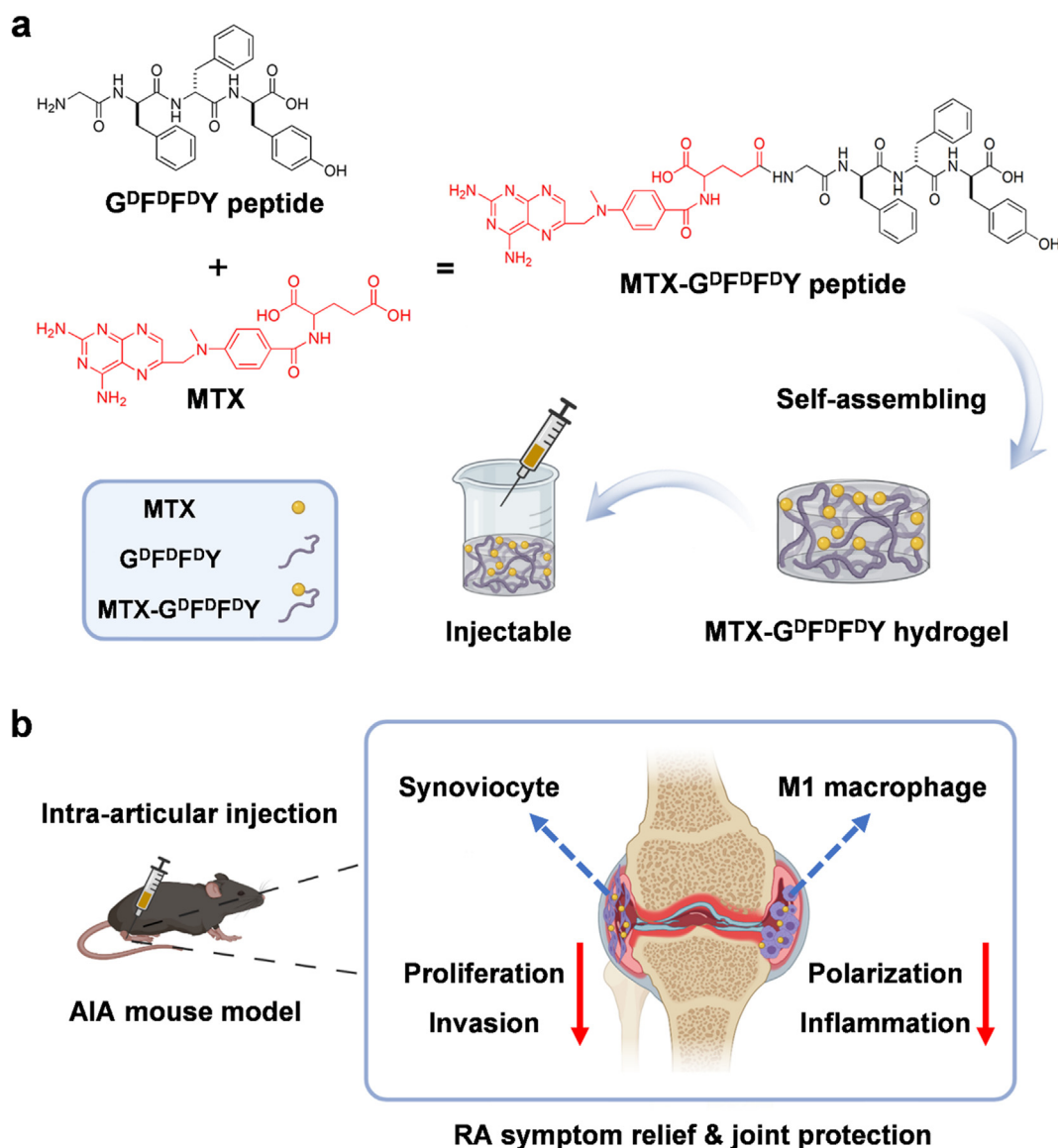
(Shanghai, China). Cy5.5 NHS ester was obtained from APEX BIO (USA). ELISA kit for IL-6 was bought from MSKBIO (China). Matrigel was bought from Corning (USA). Tubulin, iNOS, IL-6, and TNF- α antibodies used in western blot were purchased from Abcam (ab7291, ab178945, ab259341, and ab215188, respectively). In immunofluorescence staining, F4/80 was obtained from Bioss (bsm-34028 M), iNOs was obtained from Proteintech (18985-1-AP), CD206 was obtained from Abcam (ab64693), CD31 was brought from Servicebio (GB11063-2). DAPI was obtained from Beyotime Biotechnology (Shanghai, China). Commercially available reagents were used without further purification.

2.2. Preparation of Nap-GFFY, Nap-G^DF^DF^DY, and MTX-loaded hydrogels

The sequence of the peptide was 2-naphthoacetic (Nap) acid-glycine (G) -phenylalanine (F) -phenylalanine (F) -tyrosine (Y) (termed Nap-GFFY). Using 2-chlorotrityl chloride resin, our peptide was synthesized from the C' to the N' of the peptide chain by standard solid phase peptide synthesis (SPPS) [26]. The peptide were further purified by reverse-phase high performance liquid chromatography (HPLC) using a C18RP column with MeOH (0.1% of TFA) and water (0.1% of TFA) as eluent. To form the hydrogels, 5 mg of the purified peptide was dissolved in 500 μ L of PBS buffer containing Na₂CO₃ (pH = 7.4). The peptide solutions were heated by an alcohol lamp for 30 s, and then the peptide solutions were allowed to cool down at room temperature [27]. After this heating-cooling process, the peptides could self-assemble into hydrogels within approximately 2 min. Noted that the hydrogels can be also prepared by heating the peptide solutions in a water bath (100 °C, 30 s) and then cooling down at room temperature. After this heating-cooling process, the peptides could self-assemble into hydrogels within approximately 2 min. D-configuration Nap-G^DF^DF^DY hydrogel was prepared following the same protocol by using D-configuration amino acids. To prepared MTX loaded hydrogels, MTX was reacted with deaminated glycine at a 1:1 M ratio during SPPS. Then the resultant hydrogels (termed MTX-GFFY and MTX-G^DF^DF^DY) were obtained following the same method mentioned above. The MTX loading efficiency was calculated based on the amount of MTX in the raw materials and purified MTX-conjugated peptides. In 1 mmol MTX-GFFY or MTX-G^DF^DF^DY, the use of MTX was 908.9 mg. After purification and freeze-drying, MTX content in the peptide was determined to be 312.97 mg. The MTX loading efficiency was calculated to be 34.43%. In addition, Cy5.5-GFFY and Cy5.5-G^DF^DF^DY were prepared (Figure S1). Briefly, NH₂-GFFY-COOH or NH₂-G^DF^DF^DY-COOH was dissolved in DMSO and pH of the mixture was adjusted to 8–9. Then Cy5.5-NHS Ester was added into the peptide mixture at a mass ratio of 1:1.2 and the mixture was stirred at room temperature for 24 h in the dark.

2.3. Characterization of the hydrogels

HR-MS were used to characterize the peptides. Transmission electron microscopy (TEM) were used to observe the morphology of the hydrogels. Fluorescence spectra was obtained to investigate the molecular arrangements of hydrogels. The secondary structures were analyzed by circular chromatography scanner. Stability and sustained drug release were performed by reverse phase high performance liquid chromatography (HPLC) according previous reported methods [28,29]. Briefly, 1 mg of the peptides were dissolved in 5 mL PBS and proteinase K was (3.2 units/mL). The hydrogels were incubated at 37 °C. At each time point, 500 μ L of the samples were taken out and analyzed by the HPLC system (LUMTECH HPLC, Germany) using a C18RP column with MeOH (0.05% of TFA) and water (0.05% of TFA) as the eluents. Rheology test was performed using AR 2000ex (TA instrument) system. 40 mm parallel plates were used, and the gap was set to be 500 μ m. After the heating/cooling process and the formation of the hydrogels, the samples were transferred to the plat immediately. For frequency sweep, the region of 0.1–100 rad/s and the strain of 1% were chosen.



Scheme 1. Schematic illustration for the synthesis of MTX-G^DF^DF^DY hydrogels and their application in rheumatoid arthritis (RA) therapy. (a) MTX are conjugated with G^DF^DF^DY peptides through the reaction between carboxyl groups in MTX and the deaminated glycine in peptides. The resultant MTX-G^DF^DF^DY peptides can form injectable hydrogels via π - π stacking. (b) After being intra-articularly injected into the knee joints of adjuvant-induced arthritis (AIA) mice, the hydrogels can constantly release MTX during biodegradation, and thus inhibit not only the proliferation and invasion of synoviocytes, but also the polarization of proinflammatory M1 type macrophages, achieving a highly efficient RA therapy by reducing joint inflammation and destruction.

2.4. Cytotoxicity

Cell viability of the hydrogels toward mouse fibroblast (L929), human umbilical vein endothelial cell (HUVEC), RA synovial fibroblast (RA-FLS), and macrophage cell line RAW264.7 (10^4 cells per well) were evaluated by using a standard 3-(4,5-dimethyl-2-thiazolyl)-2,5-diphenyl-2-H-tetrazolium bromide (MTT) assay (Solarbio, China). Cells were cocultured with Nap-GFFY, Nap-G^DF^DF^DY, MTX-GFFY, MTX-G^DF^DF^DY, and MTX with various concentrations (200, 100, 50, 10, 5, 0 μ M), respectively, for 48 h. Then MTT assay was performed and the absorbance at 490 nm was measured using a microplate reader. Cell viability was also evaluated by Live/dead staining. After cocultured with the hydrogels or MTX (100 μ M) for 48 h cells were stained with Calcein AM/PI staining kit (Sigma, USA) and then observed by a fluorescence microscope (Leica, Germany).

2.5. Cell migration and invasion

Cell migration test was carried out by scratch test. RA-FLS were first starved for 12 h and then mixed with the hydrogels or MTX solution (100 μ M, 2 mL). Noted that the hydrogels prepared from 100 μ M of peptides were flexible. Then they were injected into well plates and cultured for 48 h. Afterwards, a straight line was scratched on the cells in each well. Then cell migration rate was calculated according to the cell healing area after additional 12 and 24 h of cocultured.

Cell invasion was performed by using a transwell system (Corning, USA). After starved for 12 h, RA-FLS were mixed with the hydrogels or MTX solution (100 μ M, 500 μ l). Then they were seeded in the upper chamber with serum-free growth medium and 100 μ l 12.5% Matrigel. Then RA-FLS were seeded in the upper chamber with serum-free growth medium and 100 μ l 12.5% Matrigel. Medium containing 20% FBS was

added in the lower chamber as the chemoattractant. After an additional culture of 24 h, the upper chambers were taken out, stained by 2% crystal violet (Solarbio, China), and observed under a microscope (Leica, Germany).

2.6. Anti-inflammatory properties of the hydrogels

To study the anti-inflammatory properties of the hydrogels, we observed the effects of the hydrogels on macrophage polarization. Mice macrophage cell line RAW 264.7 were induced into proinflammatory M1 type macrophages by treated with 1% w/v lipopolysaccharide (LPS)-containing media for 24 h. Then the M1 macrophages were mixed with 100 μ M of Nap-GFFY, Nap-G^DF^DF^DY, MTX-GFFY, MTX-G^DF^DF^DY, and MTX. After cultured for an additional 24 h, the culture medium and RAW 264.7 cells were collected from the different groups, respectively. The contents of IL-6 in the culture media were measured using an ELISA kit according to the manufacturer's introductions. Moreover, immunofluorescence staining of iNOS and CD206 was also performed on RAW264.7 cells. Total RNA and proteins of the M1 macrophages were extracted with TRIzol (Invitrogen, USA) and Cell Lysis Buffer (Abcam, USA), respectively. The relative expression levels of macrophage polarization genes including iNOS, IL-6, and TNF- α (M1 markers) were analyzed by real-time quantitative polymerase chain reaction (RT-qPCR) [30]. The absorbance was measured at 450 nm using a microplate reader. Proteins of M1 markers (iNOS, IL-6, and TNF- α) were detected by western blot assay. Tubulin was used as the internal reference. Bradford assay was carried out to measure the protein concentration. Proteins were then mixed with loading buffer, denaturized, and loaded on 10% w/v SDS-polyacrylamide gel (Beyotime, China). Then proteins were transferred from separation gel to concentration gel and were transferred to PVDF membrane (Merck Millipore, USA) using Trans-Blot® SD Semi-Dry Electrophoretic Transfer Cell (Bio-Rad, USA). Next, the membranes were probed with primary antibodies (Abcam, USA) overnight at 4 °C, washed with TBST, and reacted with secondary antibodies for 120 min at room temperature. Finally, the membranes were then visualized using a chemiluminescence detection system (GE, USA).

2.7. Establishment of adjuvant-induced arthritis (AIA) mice model and treatments

All animal studies were approved by the Animal Laboratory Center of Zhujiang Hospital, Southern Medical University (No. LAEC-2020-092). Male eight-week-old C57BL/6 mice were purchased from Guangzhou Animal Experiment Center. To establish AIA mice model, mice were induced by subcutaneous injection of 1% w/v complete Freund's adjuvant (Sigma-Aldrich, USA) in the fore underarm. One week later, a same dose of incomplete Freund's adjuvant (Sigma-Aldrich, USA) was injected subcutaneously into both hind pads of the mice. After an additional 1 week of booster immunization, the AIA mice were randomly assigned into 7 groups ($n = 5$). Each mouse was intra-articular injected with 20 μ L of PBS, Nap-GFFY, Nap-G^DF^DF^DY, MTX-GFFY, MTX-G^DF^DF^DY, and MTX on the both knees twice a week for 4 weeks. The hydrogels were prepared from 10.342 mM of peptides. Mouse dose of MTX was calculated based on the human equivalent dose according to a previous report [31].

2.8. In vivo therapeutic effects of the hydrogels

Clinical arthritis severity score was recorded according to our previous study (Table S2) [32]. Knee joint diameter was measured using a vernier caliper every week. Skin temperature of the hind paws was recorded by an infrared camera (FLIR, USA) on the 28th day after treatments. In addition, serums of mice treated with PBS or MTX-G^DF^DF^DY hydrogels were collected. The serum inflammatory cytokines (IL-6 and TNF- α) were detected by using ELISA kits according to the manufacturer's introductions.

2.9. Histological study

The mice were sacrificed on day 28 after treatments. The knee joints were collected, fixed with 4% paraformaldehyde overnight, followed by decalcification with EDTA decalcified solution for 30 days. Then safranin-O/fast green (Beyotime Biotechnology, China) and hematoxylin-eosin (H&E, Beyotime Biotechnology, China) staining were performed. Mankin pathological scores (Table S3-S5) were used to evaluate inflammation and cartilage destruction.

For immunohistochemistry of M1 macrophages, tissue sections were dewaxed, and stained with primary antibodies against IL-6 (Abcam, USA). After stained with secondary antibodies, the tissue sections were observed by a microscope.

2.10. In vivo stability of the hydrogels

To study the stability and retention time of the hydrogels, 20 μ L of Cy5.5-GFFY or Cy5.5-G^DF^DF^DY hydrogels were intraarticularly injected into the knee joints of AIA mice. At day 0, 1, 5, 7, and 10, mice were imaged using an *in vivo* fluorescence imaging system (FX PRO, BRUKER, Germany) with an excitation wavelength of 630 nm and an emission wavelength of 700 nm. The images were analyzed using the BRUKER Molecular Imaging Software.

2.11. Immunofluorescence staining

The knee joint sections were incubated with CD31, F4/80, CD206, and iNOS antibodies (1:300) at 4 °C overnight, respectively. Afterwards, samples were incubated with secondary Alexa Fluor 488 antibody or Alexa Fluor cy3 (1:8000; Abcam, UK) for 2 h at room temperature. Nuclei were stained with DAPI (Beyotime, China). Images were captured by a Leica fluorescence microscope.

2.12. In vivo toxicity of the hydrogels

After intra-articular injection of the hydrogels, body weight of the mice was measured every 3 days. After 28 days of treatments, liver and kidney function of the mice were detected by blood biochemistry detection kit (Service, China) in an automatic analyzer (Rayto Biotechnology, China). Moreover, liver and kidney tissues were collected and stained with H&E staining for histological study.

2.13. Statistics analysis

SPSS 20.0 software (IBM, USA) was used for statistics analysis. Independent-sample *t*-test or ANOVA test was used for data comparison. $p < 0.05$ represents a statistically significant difference. All data were presented as mean \pm standard deviation (mean \pm SD).

3. Results and discussion

3.1. Preparation and characterization of the hydrogels

We synthesized classic L-configuration Nap-GFFY peptide via a classic solid-phase peptide synthesis (SPPS) method. D-configuration Nap-G^DF^DF^DY peptide was prepared using the same method but replacing the corresponding L-amino acids with D-amino acids. MTX was conjugated into the peptides through the reaction between carboxyl groups in MTX and the amino terminus of glycine in peptides to produce MTX-GFFY and MTX-G^DF^DF^DY (Fig. 1a). The loading efficiency of MTX in the peptide was calculated to be 34.43%. The molecular structures of these synthetic peptides were confirmed by HR-MS (Figure S2). We used 10.317 mM (1 wt%) peptides to test whether these peptides can self-assemble into hydrogels. As shown in Fig. 1b (inserted images), all the compounds could effectively form stable transparent hydrogels by a heating-cooling process. The dynamic gelation process showed that MTX-G^DF^DF^DY

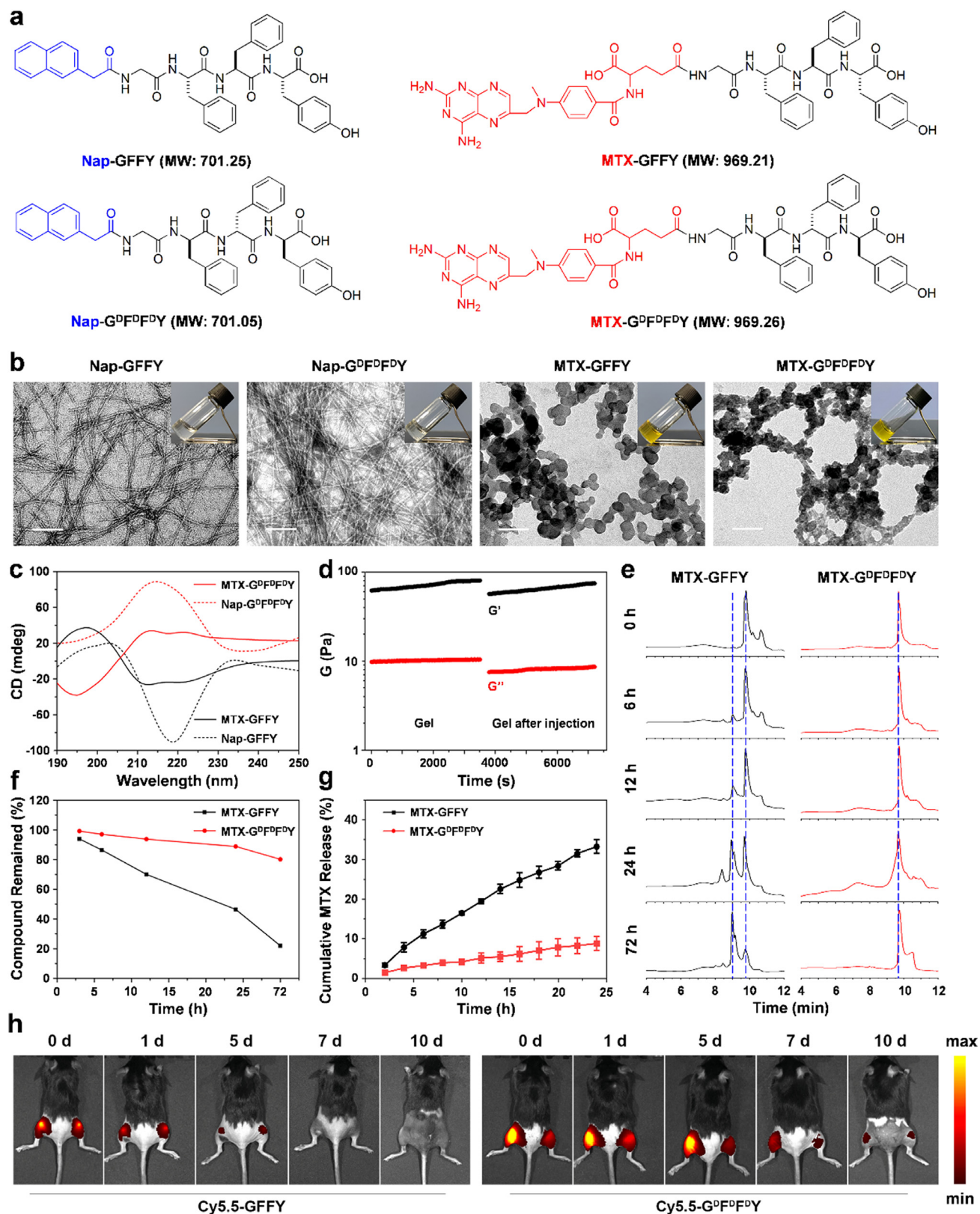


Fig. 1. Design and characterization of the hydrogels. (a) The chemical structures of Nap-GFFY, Nap-G^DF^DF^DY, MTX-GFFY, and MTX-G^DF^DF^DY. (b) TEM images of the hydrogels. Inset images: hydrogels formed by 10.317 mM (1 wt%) of different peptides in PBS. Scale bar = 100 nm. (c) Circular dichroism (CD) revealed the chirality of the hydrogels. (d) Gelation behavior of MTX-G^DF^DF^DY hydrogels before and after injection. (e) HPLC analysis of the hydrogels exposed to proteinase K. (f) Compound remained rate calculated from (e). (g) Cumulative MTX release from MTX-GFFY and MTX-G^DF^DF^DY hydrogels in PBS within 24 h ($n = 3$). (h) Fluorescence imaging of the mice after the intra-articular injection of Cy5.5-GFFY or Cy5.5-G^DF^DF^DY hydrogel at day 0, 1, 5, 7, and 10.

hydrogel became stable within 2 min (Figure S3).

Transmission electron microscopy (TEM) images revealed that ordered nanostructures were formed in the hydrogels (Fig. 1b). Specifically, Nap-GFFY and Nap-G^DF^DF^DY hydrogels presented long and flexible nanofibers with an average diameter of 8 ± 2 nm. In comparison, MTX-GFFY and MTX-G^DF^DF^DY hydrogels exhibited a net-like structure where ball-like structures were stacked on the network. The morphology of hydrogels prepared from 100 μ M of peptides was also investigated. The laser beam (Figure S4) indicated the formation of homogeneous micelles and the TEM image (Figure S5) suggested the 100 μ M of peptides had self-assemble into nanofibers.

To investigate the molecular arrangements in the solution-gel process of hydrogels, fluorescence spectra was obtained (Figure S6). After self-assembled into hydrogels, the peak value of the identical amino acid sequence redshifted from 330 nm to 342 nm in Nap-GFFY and Nap-G^DF^DF^DY, and shifted from 460 nm to 480 nm in MTX-GFFY and MTX-G^DF^DF^DY. This indicated that the π - π stacking effect of benzene ring was enhanced after self-assembly, enabling the peptides to form nanofibers and then wrap water molecules to form hydrogels. Subsequently, secondary structures of the hydrogels were analyzed by circular chromatography scanner to further understand the molecular arrangements and the driven forces (Fig. 1c). Nap-GFFY hydrogels had a positive band at 205 nm and a negative band at 218 nm, indicating a β -sheet conformation. Nap-G^DF^DF^DY hydrogels exhibited a positive peak at approximately 215 nm in the PBS buffer solution. The mirror pattern of L-configuration hydrogels and its corresponding D-configuration hydrogels reflects their chirality. MTX-GFFY hydrogels presented a peak near 195 nm and two troughs near 212 nm and 222 nm, which could be assigned to α -helix secondary structure. Similarly, the CD spectra of MTX-G^DF^DF^DY hydrogels was completely opposite to MTX-GFFY, confirming the chirality of enantiomeric pairs of these two hydrogels. According to the CD results, we speculated that the differences in secondary structure of hydrogels might attribute to their discrepancies in nanostructures (determined by TEM images). Nap-terminated hydrogels have β -sheet secondary structure, thus they showed a certain rigid fibrous structure in TEM. The nanostructure was relatively loose in MTX-terminated hydrogels due to their α -helix secondary structure.

The mechanical characteristics of the hydrogels were analyzed by rheology. As shown in Figure S7, the storage modulus value (G') of the resultant four types of hydrogels (10.317 mM) was higher than the loss modulus value (G''), suggesting the formation of true hydrogels. In the frequency range of 0.1–100 rad/s, both G' and G'' showed weak frequency dependences, indicating that these hydrogels were composed of elastic networks. Compared with Nap-derived peptides, MTX-derived peptides have lower G' and G'' values. The difference between G' and G'' became smaller, indicating that the mechanical strength of the MTX-loaded hydrogels was slightly weaker. Further, we tested the rheological properties of MTX-G^DF^DF^DY hydrogel before and after injection (Fig. 1d). After the hydrogel was injected, it became a thick fluid for a period of time and returned to gel after 5 min. Compared to the state before injection, G' and G'' slightly decreased but the value of G'' was still one magnitude less than that of G' , suggesting that the recovered material remained a true hydrogel.

Stability and sustained drug release are also important for a drug delivery system. Biostability of the MTX-loaded hydrogel was tested by exposing them to proteinase K at 37 °C. We found that MTX-GFFY hydrogel became flowable after 1-day and gradually disintegrated over time. By contrast, D-configuration MTX-G^DF^DF^DY hydrogel were stable in vitro for approximately 5 days (Figure S8). HPLC spectra (Fig. 1e) showed that the peak of MTX-GFFY gradually decreased after the addition of proteinase K. However, the peak of MTX-G^DF^DF^DY had no obvious change during incubation, suggesting that D-configuration hydrogels were more stable than L-configuration hydrogels. We calculated the degradation curve from HPLC results and found that the remained compound of MTX-GFFY and MTX-G^DF^DF^DY hydrogels was 45% and 90%

after 24 h, and 20% and 80% after 3 days, respectively (Fig. 1f). Further, we investigated the *in vivo* stability and retention time of the hydrogels in the knee joints of AIA mice. As shown in Fig. 1h, both Cy5.5-GFFY and Cy5.5-G^DF^DF^DY hydrogels were observed at 1-day post-injection. The fluorescence intensity of the hydrogels gradually decreased overtime. At day 7, Cy5.5-GFFY hydrogels were barely detected. By contrast, Cy5.5-G^DF^DF^DY hydrogels exhibited a stronger fluorescence intensity relative to Cy5.5-GFFY hydrogels in joints at all time intervals and could be observed for approximately 10 days. Our results are consistent with previous reports that self-assembled peptides constructed with D-amino acid shows an increased resistance to enzymatic hydrolysis compared with L-configuration peptides [33]. Next, drug release of 1%wt MTX-loaded hydrogels was evaluated. As shown in Fig. 1g, MTX constantly released from both hydrogels during the 24 h without burst release. Moreover, MTX releasing rate of D-configuration hydrogels was approximately 8% while it was 32% in L-configuration hydrogels. Hence, MTX-G^DF^DF^DY hydrogels might be more efficient than MTX-GFFY hydrogels for sustained drug delivery to enhance therapeutic effect of MTX *in vivo*.

3.2. Effects of the hydrogels on cell proliferation, migration, and invasion

We evaluated the cytotoxicity of Nap-GFFY and Nap-G^DF^DF^DY hydrogels toward normal cell lines (L929 and HUVEC) and RA synovial fibroblasts (RA-FLS). As shown in Fig. 2a-c, the hydrogels had almost no inhibiting effect on cell proliferation. Then we compared the cytotoxicity of MTX-GFFY and MTX-G^DF^DF^DY hydrogels (Fig. 2e-g). In MTX-GFFY groups, an obvious cytotoxicity toward normal L929 and HUVEC cells were found when the concentration was more than 5 μ M, whereas they showed mild effects on RA-FLS even with a high concentration of 100 μ M. Similar results were also observed in macrophage cell line RAW264.7 (Figure S9). By contrast, MTX-G^DF^DF^DY reduced the cytotoxicity on normal cells as compared to MTX-GFFY groups. Noted that MTX-G^DF^DF^DY hydrogels exhibited a selective inhibiting effect on RA-FLS that they significantly inhibited RA-FLS proliferation with a concentration of 50 μ M.

We further confirmed cytotoxicity of the hydrogels by live/dead staining (Figure S10). Similarly, cells cocultured with Nap-GFFY and Nap-G^DF^DF^DY hydrogels were all alive (green fluorescence). After loaded with MTX, less L929 and HUVEC cells were dead (red fluorescence) in MTX-G^DF^DF^DY groups compared to MTX-GFFY and free MTX groups. As to RA-FLS, MTX-G^DF^DF^DY hydrogels significantly enhanced the ratio of dead cells/live cells, indicating their selective inhibiting effects on RA synoviocytes. These live/dead staining results are in accordance with the MTT data and previous reports that D-configuration supramolecular hydrogels have a better biocompatibility and can increase drug selectivity compared to natural L-configuration hydrogels [17]. Therefore, our MTX-loaded hydrogels, especially MTX-G^DF^DF^DY, could not only reduce drug toxicity to normal cells, but also enhance the inhibiting effect on the proliferation of RA synoviocytes.

In addition to synovial hyperplasia, migration and invasion of synovial fibroblasts can erode cartilage surface and destroy joint structure, playing an important role in RA pathology [34]. We studied the effect of the hydrogels on cell migration of RA-FLS cells by wound-healing assay (Fig. 2h). Wound-healing rate in Nap-GFFY and Nap-G^DF^DF^DY groups were similar compared to control group. In MTX groups, wound-healing rates were 50% and 100% at 12 h (Figs. 2j) and 24 h (Fig. 2k), respectively. Impressively, the MTX-loaded hydrogels significantly inhibited the migration of RA-FLS. After 24 h of coculture, the wound-healing rates were only 50% and 40% in MTX-GFFY and MTX-G^DF^DF^DY hydrogel groups, respectively. However, cell scratches were completely healed in the other groups.

Then we verified the effect of the hydrogels on the invasion of RA-FLS cells in vitro using a transwell system. As shown in Fig. 2i, a large number of RA-FLS invaded into the lower chamber in control, Nap-GFFY, and

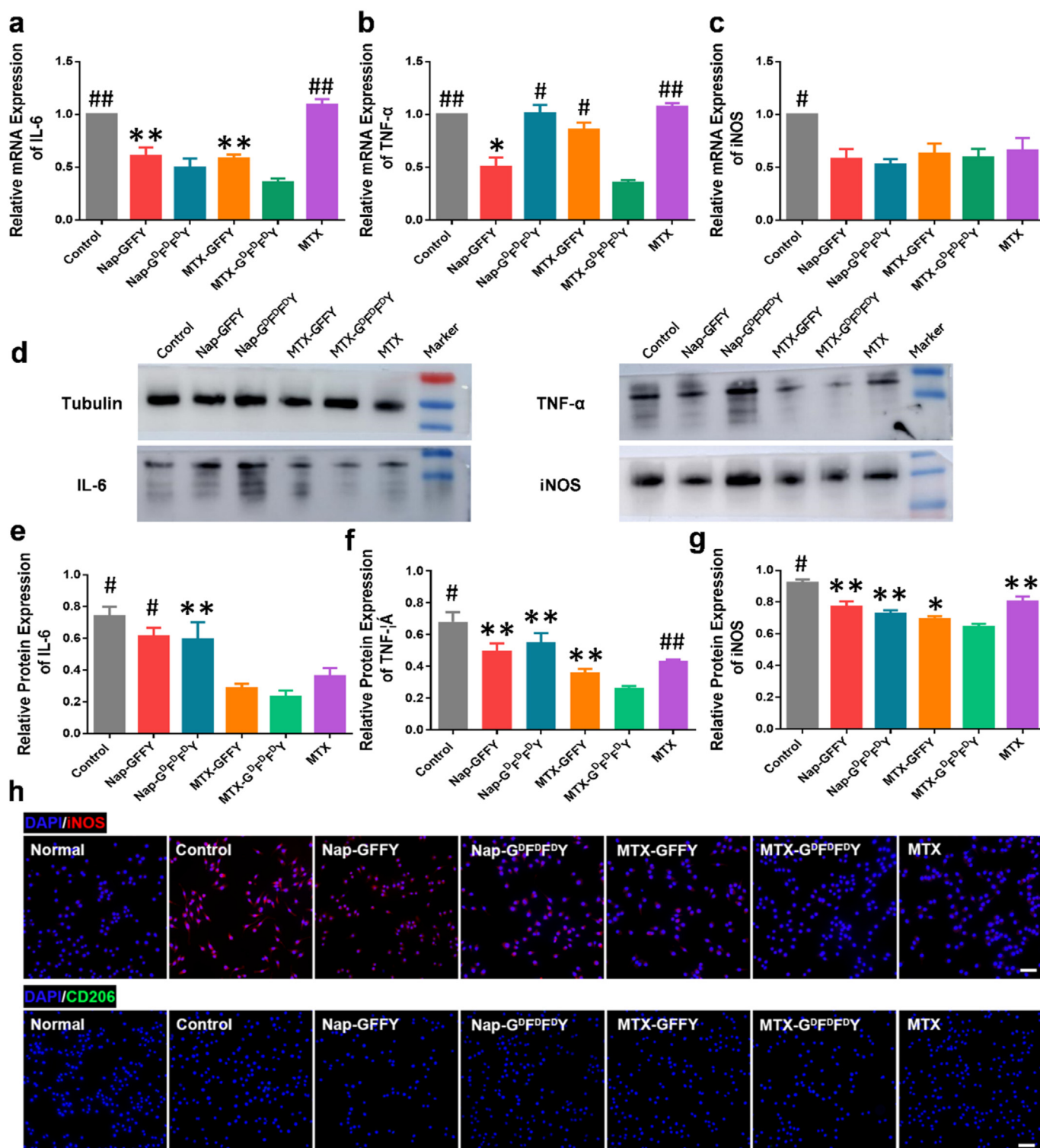


Fig. 3. Anti-inflammatory effect of the hydrogels on M1 type macrophages. Relative mRNA expression of M1 macrophages markers IL-6 (a), TNF-α (b), and iNOS (c) on LPS-induced RAW264.7 cells ($n = 3$). (d) Western blot of M1 macrophages markers on RAW264.7 with different treatments. Tubulin was set as the internal reference. (e–g) Quantitative analysis of protein bands in (d) based on optical density ($n = 3$). (h) Immunofluorescence staining of M1 macrophages markers (iNOS) and M2 macrophages markers (CD206) on RAW264.7 with different treatments. Data are presented as means \pm SD. * $p < 0.05$, ** $p < 0.01$, *** $p < 0.001$, **** $p < 0.0001$ compared to MTX-G^{DFDFDY} group. Scale bar = 50 μ m.

Nap-G^DF^DF^DY groups. Free MTX inhibited approximately half of the crossed RA-FLS. In contrast, cell numbers were obviously decreased in MTX-GFFY and MTX-G^DF^DF^DY groups (Figure 2f). Hence, MTX-GFFY and MTX-G^DF^DF^DY hydrogels could effectively inhibit the migration and invasion of RA-FLS, suggesting they might have a better therapeutic effect *in vivo*.

3.3. Anti-inflammatory effects of the hydrogels

Synovial inflammation is the main cause of RA symptoms such as pain and joint swelling [1].

MTX can relieve RA symptoms by its immuno-regulatory capacity in

the inflammatory synovial tissues [35,36]. Clinical evidences reveal that the number of macrophages is significantly increased in synovial tissue of RA patients [37]. Specifically, proinflammatory M1-type macrophages was significantly activated [38]. This kind of immune cells not only secrete proinflammatory cytokines such as TNF- α , IL-6, and IL-1 β , but also accelerate the degradation of cartilage extracellular matrix [39]. To study the anti-inflammatory effects of the hydrogels, we investigated gene and protein expression in M1 macrophages. We induced macrophage cell line RAW264.7 into M1 macrophages by stimulating them with lipopolysaccharide (LPS) [40,41]. Then M1 macrophages were mixed with different hydrogels (100 μ M, 2 mL) and cultured in well plates for an additional 24 h. The relative gene expression of M1 markers (IL-6, TNF- α ,

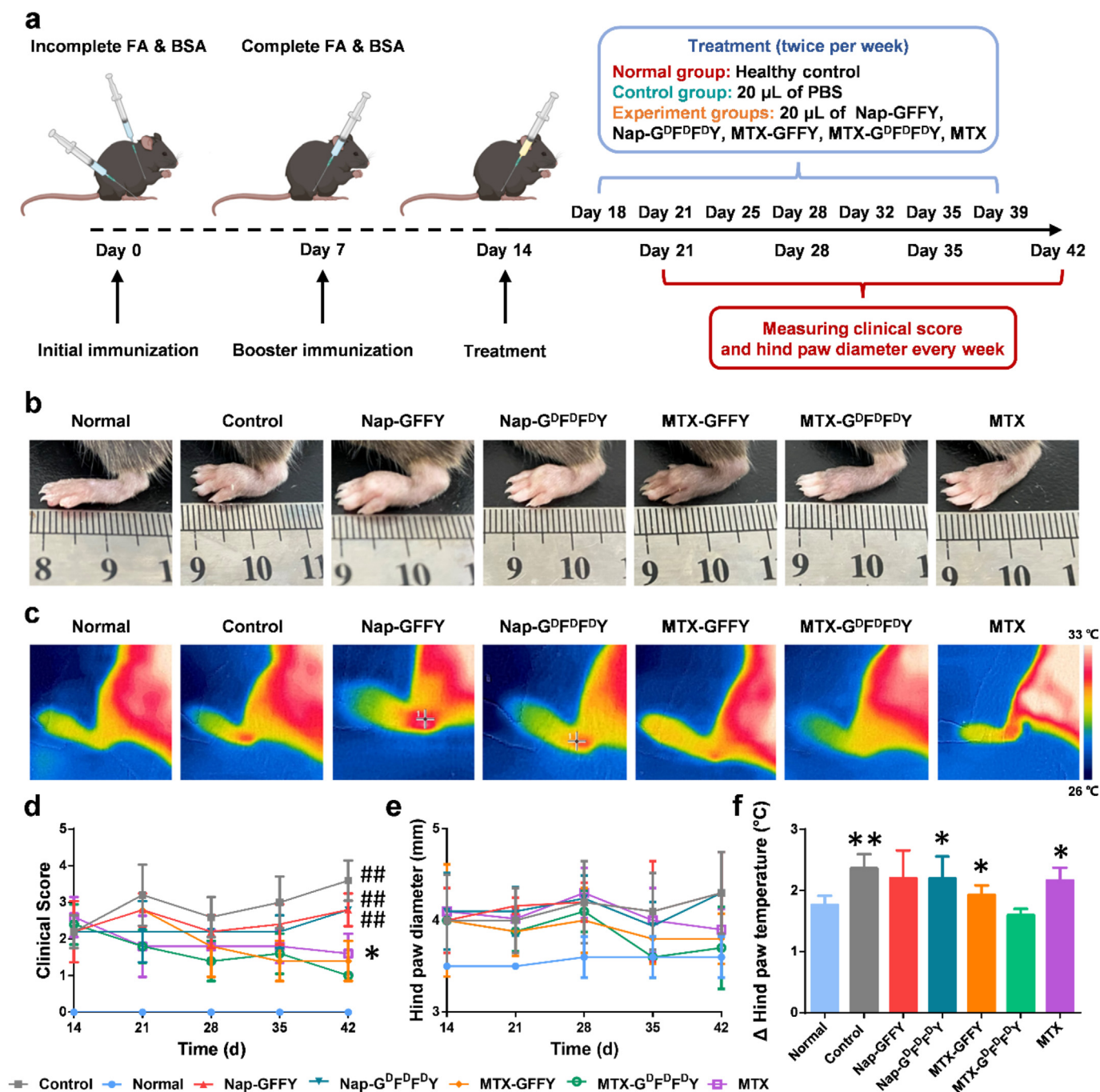


Fig. 4. Therapeutic effect of the hydrogels on AIA mice model. (a) Schematic illustration for the establishment of AIA mice model and the therapeutic regimen. (b) Representative photos of hind paws of mice after 28 days of different treatments. (c) Representative infrared photos of ankle skin temperature of mice after treatments. (d) Dynamic clinical score of the mice (e) Dynamic changes of hind paw diameter of mice in different treatment groups. (f) Changes of hind paw temperature of mice after treatments. Data are presented as means \pm SD ($n = 5$). * $p < 0.05$, ** $p < 0.01$, # $p < 0.001$, ## $p < 0.0001$ compared to MTX-G^DF^DF^DY group. Scale bar = 500 μ m.

and iNOS) is presented in Fig. 3a-c. Interestingly, we found that Nap-GFFY, Nap-G^DF^DF^DY, and MTX-loaded hydrogels decreased the expression level of IL-6 and iNOS compared to control group (LPS), whereas the anti-inflammatory effect of MTX was not obvious. Moreover, MTX-G^DF^DF^DY hydrogels exhibited the strongest anti-inflammatory effects that all marker genes of M1 macrophages were significantly down-regulated. The ELISA results (Figure S11) showed that MTX-loaded hydrogels reduced the secretions of inflammatory factor IL-6 from M1 macrophages to the culture media.

We further detected protein expression in M1 macrophages by western blotting (Fig. 3d). Nap-GFFY and Nap-G^DF^DF^DY hydrogels slightly inhibited the expression of M1 macrophage related proteins compared to control group (LPS). Furthermore, the MTX-loaded hydrogels significantly reduced TNF- α and IL-6 expression in M1 macrophages, and their inhibition of these inflammatory proteins was better than that of free MTX group. Notably, D-configuration MTX-G^DF^DF^DY hydrogels showed the best inhibitory effect on the expression of M1 macrophage markers, which was consistent with the RT-qPCR results. These above-mentioned data demonstrated that MTX-loaded hydrogels could relieve inflammation through inhibiting the polarization of M1 macrophages. Immunofluorescence staining results revealed that the expression of iNOS (M1 marker) was highly expressed in RAW264.7 cells in Nap-GFFY, Nap-G^DF^DF^DY, and control groups. In contrast, the expression of iNOS significantly decreased after treated with MTX and MTX-loaded hydrogels. The D-configuration MTX-G^DF^DF^DY hydrogels showed the strongest inhibitory effect on the polarization of M1 macrophages among all groups. In addition, the expression of CD206 (M2 marker) was similar in all groups (Fig. 3h).

3.4. In vivo therapeutic effect of the hydrogels on AIA mice

The excellent anti-inflammatory ability of the hydrogels encouraged us to further explore their therapeutic effect *in vivo*. We established an adjuvant-induced (AIA) mouse model according to our previous reported methods with modifications [42]. The hydrogels were intra-articularly injected into the knee joints of AIA mice twice per week (Fig. 4a). After 4 weeks of treatment, we found that the paws of the mice in Nap-GFFY, Nap-G^DF^DF^DY, and control (PBS) groups were severely swollen compared to healthy mice (normal group), suggesting pure hydrogels had negligible therapeutic effects *in vivo*. MTX-GFFY hydrogels and free MTX showed similar effects that paw swelling was alleviated after treatment. Remarkably, intra-articular injection of MTX-G^DF^DF^DY hydrogels effectively relieved paw swelling, and thus paw diameter was the lowest among all treatment groups (Fig. 4b and e).

Joint fever is another typical symptom that reflects joint inflammation. We recorded the skin temperature of hind paws with an infrared camera on the 28th day after administration. As shown in Fig. 4c and f, skin temperatures in the control, Nap-GFFY, and Nap-G^DF^DF^DY groups reached approximately 33.5 °C, indicating that inflammation of joints in these groups was severe. The average paw temperature in MTX-GFFY, MTX-G^DF^DF^DY, and MTX group was below 33 °C. Among these treatment groups, paw temperature in MTX-G^DF^DF^DY group was 31 °C, which was similar to that of healthy mice, suggesting MTX-G^DF^DF^DY hydrogels had relieved joint inflammatory.

The dynamic clinical scores (Fig. 4d) also displayed the same trend as joint swelling and fever. The clinical index gradually decreased in MTX-loaded hydrogels and free MTX groups, while it kept rising in pure hydrogels and control groups. Further, the clinical score after MTX-

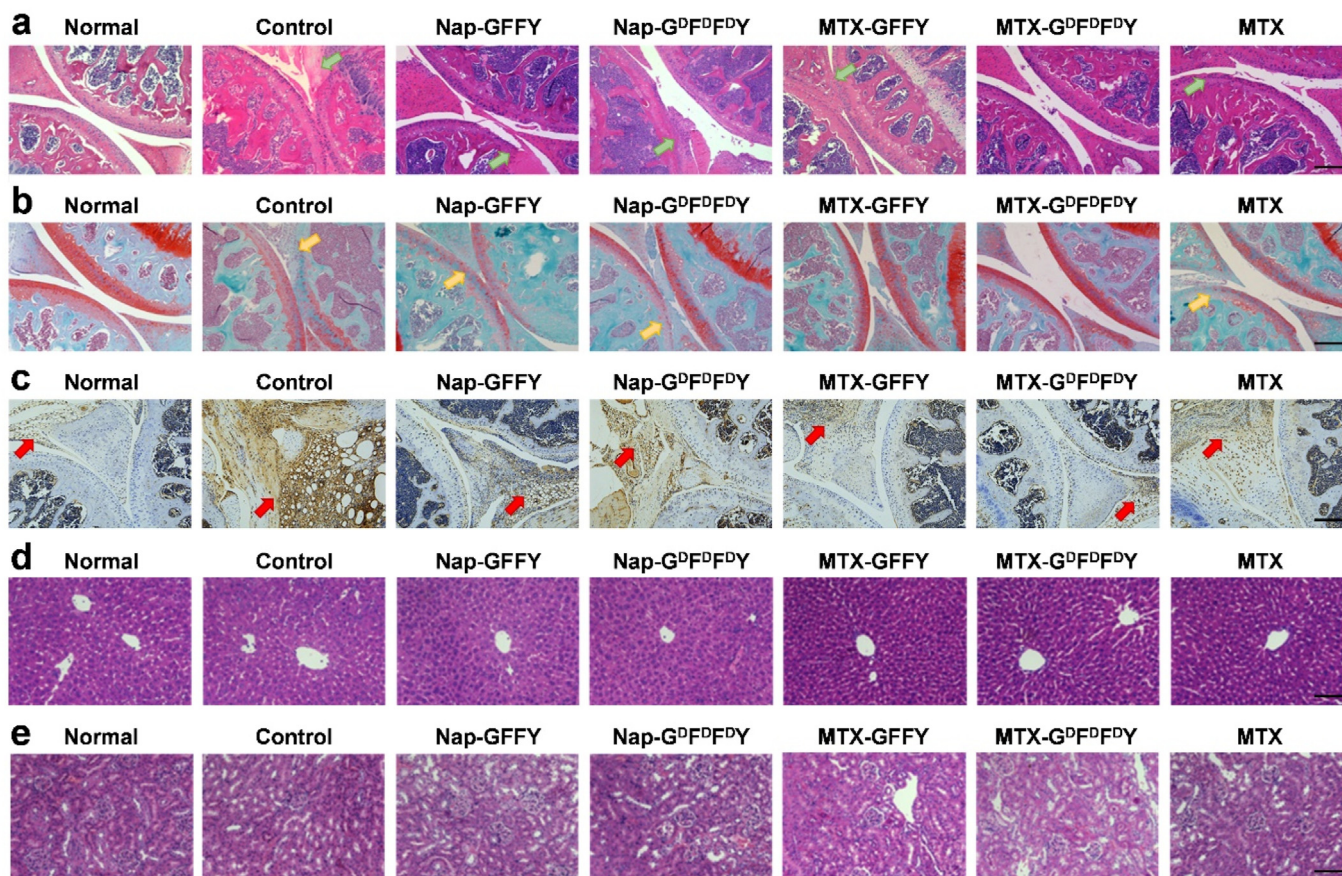


Fig. 5. Histological study on joint and organ sections of AIA mice after different treatments. (a) H&E staining of joints collected from AIA mice (green arrows represent synovial tissues). (b) Safranin-O staining of joints (yellow arrows represent cartilage tissue). (c) Expression of IL-6 (highlighted by red arrows) in synovial tissue of joints. H&E staining of liver (d) and kidney (e) after treatments. Scale bar = 200 and 100 μ m in (a–c) and (d–e), respectively.

G^DF^DF^DY treatment was the lowest among all groups after 28 days, indicating that MTX-G^DF^DF^DY hydrogels had the best therapeutic effects.

3.5. Pathological study of knee joint of AIA mice after treatments

Inflammatory synovial hyperplasia and articular cartilage destruction are the main pathological features of RA [43]. We performed H&E staining to evaluate synovial hyperplasia and joint structure of AIA mice (Fig. 5a). In control group, inflammatory synovium (green arrows) completely invaded into knee joints, causing severe joint destruction and joint space narrowing. Synovium inflammation also occurred in Nap-GFFY and Nap-G^DF^DF^DY groups but joint destruction was less than that of control group. After treated with MTX-GFFY and free MTX, synovial evasion was inhibited. Remarkably, knee joint structure was well protected and synovium inflammation was mild in MTX-G^DF^DF^DY group.

We investigated cartilage erosion by Safranin-O/fast green staining (Fig. 5b). Cartilage (yellow arrows) was only stained into pale red color in the pure hydrogel and control groups, confirming that cartilage had

been destroyed in these groups. In comparison, cartilage in AIA mice treated with MTX-loaded hydrogels was well stained and cartilage erosion was mild as compared to normal mice. We quantitatively analyzed joint pathology after different treatments using Mankin histological score (Figure S12). The scores were significantly increased in the pure hydrogel and control groups compared to normal mice. Moreover, scores in MTX-loaded hydrogel groups were significantly lower than that of MTX group, demonstrating that MTX-loaded hydrogels, particularly MTX-G^DF^DF^DY hydrogels, were more effective than free MTX in terms of inflammation inhibition and cartilage protection. Moreover, IL-6 was detected as a biomarker of local inflammation by immunohistochemistry (Fig. 5c). In control group, the expression level of IL-6 (highlighted by red arrows) in synovial tissue was significantly higher than that of the normal group. Impressively, IL-6 expression was significantly diminished after treatment of the hydrogels. In particular, the IL-6 expression level in MTX-G^DF^DF^DY group decreased to a similar level to normal group. Serum inflammatory factors (IL-6 and TNF- α) of mice were also detected after treatments of PBS or MTX-G^DF^DF^DY hydrogels (Figure S13). We found

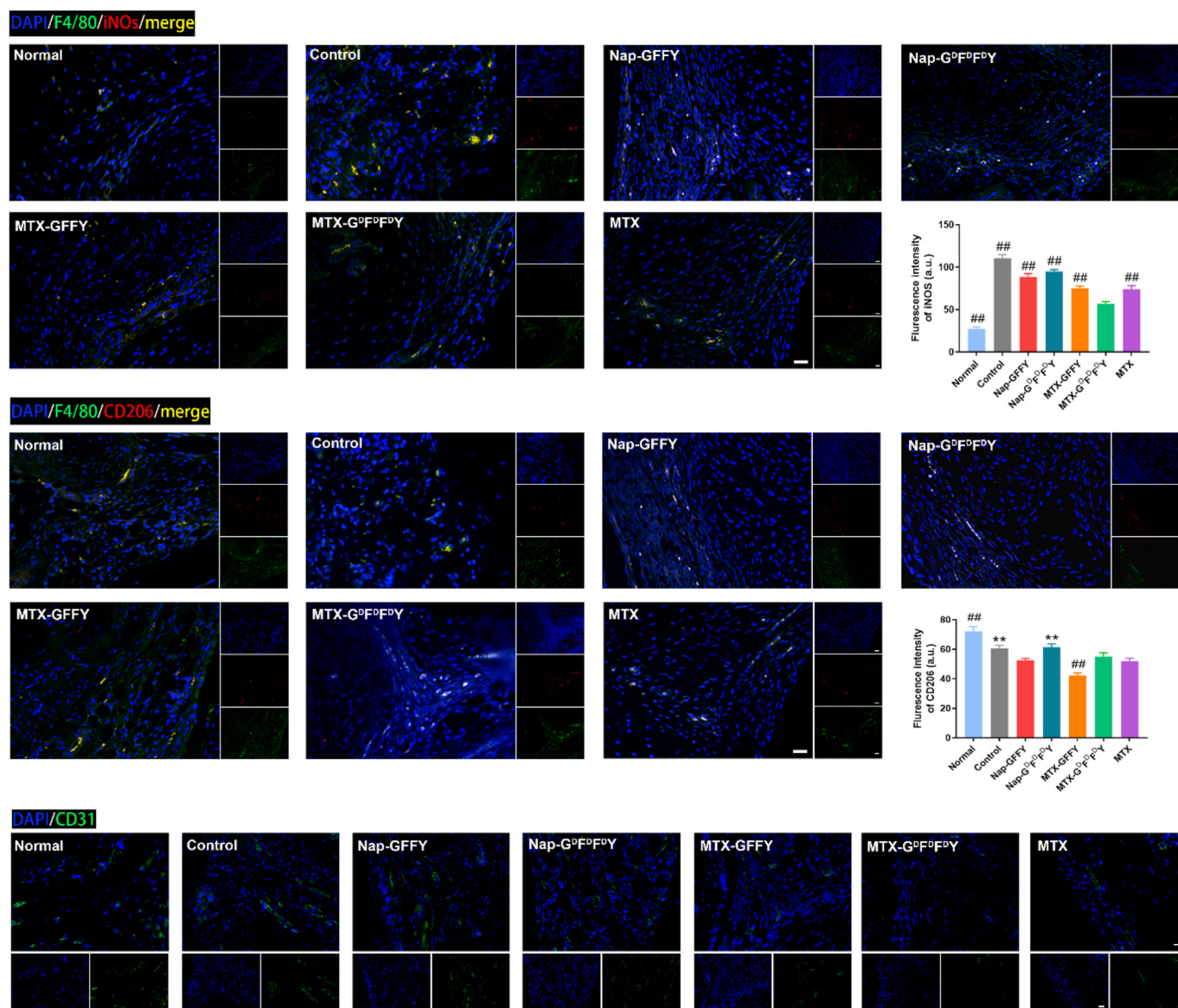


Fig. 6. Immunofluorescence staining of synovial tissues of AIA mice. Polarization of macrophages in the synovial tissues after different treatments was observed by staining of M0 macrophage marker (F4/80, green fluorescence), M1 macrophage marker (iNOS, red fluorescence; a) and M2 macrophage marker (CD206, red fluorescence; b). (c) Immunofluorescence staining of CD31 after different treatments. Data are presented as means \pm SD ($n = 3$). * $p < 0.05$, ** $p < 0.01$, # $p < 0.001$, ## $p < 0.0001$ compared to MTX-G^DF^DF^DY group. Scale bar = 20 μ m.

that the level of serum IL-6 and TNF- α were slightly lower in MTX-G^DF^DF^DY group compared to PBS group, but without statistical difference, suggesting that MTX-G^DF^DF^DY hydrogels exhibited therapeutic effects mainly through local anti-inflammatory activity.

Polarization of macrophages in the synovial tissues was evaluated by immunofluorescence staining (Fig. 6a and b). In control, Nap-GFFY, and Nap-G^DF^DF^DY groups, the expression of iNOS (red fluorescence; M1 macrophages) was stronger than that of normal group, indicating that M1 macrophages were abundant in the synovial tissues of these treatment groups. By contrast, the fluorescence signal of iNOS in MTX-GFFY, MTX-G^DF^DF^DY, and MTX groups was significantly decreased. Specifically, the fluorescence signal of iNOS was lowest in MTX-G^DF^DF^DY group among all treatment groups, demonstrating that MTX-G^DF^DF^DY hydrogels effectively inhibited the polarization of M1 macrophages *in vivo* (Fig. 6a). In addition, the expression of CD206 (red fluorescence; M2 macrophages) has no obviously difference among all groups (Fig. 6b). Therefore, MTX-G^DF^DF^DY hydrogels relieved joint inflammation mainly through inhibiting the polarization of macrophages to M1 type and maintaining them at M0 stage.

In addition, synovial pannus was visualized by immunofluorescence staining of CD31 (Fig. 6c). MTX and the MTX-loaded hydrogels inhibited neovascularization (low CD31 expression, green fluorescence) in synovial tissues of AIA mice. The fluorescence intensity of MTX-G^DF^DF^DY and MTX groups were lowest among all treatment groups (Figure S14). However, the pure hydrogels (Nap-GFFY and Nap-G^DF^DF^DY) had negligible effects on inhibiting synovial pannus compared to control group.

3.6. *In vivo* biosafety of the hydrogels

We recorded the dynamic body weight of AIA mice after injected of the hydrogels. As concluded in Figure S15, body weight of mice in all groups did not fluctuate significantly during treatments, suggesting that the hydrogels had no systematic toxicity and did not affect the growth of mice. After 28 days of treatments, we collected liver and kidney tissues from mice and evaluated them by H&E staining (Fig. 5d and e). The liver and kidney sections in all treatment groups showed no clear indication of glomerular injury, and the morphology of liver cells was normal compared to healthy mice. Moreover, blood biochemical analysis (Figure S16) demonstrated that the typical liver and kidney function indicators alanine transaminase (ALT) and creatinine (CR) of mice in all groups were within normal ranges. Hence, the hydrogels were safe *in vivo* for RA therapy and did not causes damage to liver and kidney functions.

4. Conclusion

In conclusion, we successfully synthesized a series of supramolecular polypeptide hydrogels with self-assembled, injectable, and drug delivering capacity. We showed that the D-configuration MTX-G^DF^DF^DY hydrogels exhibited better stability and longer drug releasing behavior compared to MTX-GFFY hydrogels. More importantly, MTX-G^DF^DF^DY hydrogels could not only reduced MTX toxicity to normal cells, but also effectively inhibited the invasion of RA synoviocytes and the polarization of inflammatory M1 macrophages. Consequently, MTX-G^DF^DF^DY hydrogels significantly relieved RA syndromes, including joint destruction, swelling and fever, without causing any side effects after intra-articular injection. Hence, MTX-G^DF^DF^DY hydrogels hold great potential for applications in the treatment of RA.

Credit author statement

Shaodan Ma: Writing – original draft, Methodology, Investigation, Visualization. Shunan Gu: Writing – original draft, Methodology, Investigation. Jinwei Zhang: Methodology, Investigation. Weizhong Qi: Methodology, Investigation. Zhaowei Lin: Methodology, Investigation. Weicheng Zhai: Methodology, Investigation. Jie Zhan: Methodology, Investigation. Qi Li: Conceptualization, Funding acquisition, Supervision.

Yanbin Cai: Conceptualization, Funding acquisition, Supervision, Writing – review & editing. Yao Lu: Conceptualization, Funding acquisition, Supervision, Writing – review & editing.

Declaration of competing interest

The authors declare that they have no known competing financial interests or personal relationships that could have appeared to influence the work reported in this paper.

Acknowledgement

This study was supported by National Natural Science Foundation of China (82172391, 81902198, 51973090, 31900952), Guangdong Basic and Applied Basic Research Foundation (2020A1515010398, 2019A1515011706), China National Postdoctoral Program for Innovative Talents (BX20190150), China Postdoctoral Science Foundation (2019M662980), and President Foundation of Zhujiang Hospital, Southern Medical University (yzjj2018rc09).

Appendix ASupplementary data

Supplementary data to this article can be found online at <https://doi.org/10.1016/j.mtbio.2022.100296>.

References

- [1] J.S. Smolen, D. Aletaha, I.B. McInnes, Rheumatoid arthritis, *Lancet* 388 (2016) 2023–2038, [https://doi.org/10.1016/S0140-6736\(16\)30173-8](https://doi.org/10.1016/S0140-6736(16)30173-8).
- [2] D.L. Scott, F. Wolfe, T.W. Huizinga, Rheumatoid arthritis, *Lancet* 376 (2010) 1094–1108, [https://doi.org/10.1016/S0140-6736\(10\)60826-4](https://doi.org/10.1016/S0140-6736(10)60826-4).
- [3] J.A. Singh, K.G. Saag, S.J. Bridges, E.A. Akl, R.R. Bannuru, M.C. Sullivan, E. Vaysbrot, C. McNaughton, M. Osani, R.H. Shmerling, J.R. Curtis, D.E. Furst, D. Parks, A. Kavanaugh, J. O'Dell, C. King, A. Leong, E.L. Matteson, J.T. Schousboe, B. Drevlow, S. Ginsberg, J. Grober, C.E. St. E. Tindall, A.S. Miller, T. McAlindon, American college of rheumatology guideline for the treatment of rheumatoid arthritis, *Arthritis Care Res.* 68 (2015) 1–25, <https://doi.org/10.1002/acr.22783>, 2016.
- [4] C. Mazaud, L. Fardet, Relative risk of and determinants for adverse events of methotrexate prescribed at a low dose: a systematic review and meta-analysis of randomized placebo-controlled trials, *Br. J. Dermatol.* 177 (2017) 978–986, <https://doi.org/10.1111/bjd.15377>.
- [5] A. Strangfeld, J. Listing, P. Herzer, A. Liebhaber, K. Rockwitz, C. Richter, A. Zink, Risk of herpes zoster in patients with rheumatoid arthritis treated with anti-TNF- α agents, *JAMA* 301 (2009) 737–744, <https://doi.org/10.1001/jama.2009.146>.
- [6] V.M. Gouveia, J. Lopes-de-Araújo, L.S. Costa, C. Nunes, S. Reis, Hyaluronic acid-conjugated pH-sensitive liposomes for targeted delivery of prednisolone on rheumatoid arthritis therapy, *Nanomedicine* 13 (2018) 1037–1049, <https://doi.org/10.2217/nmm-2017-0377>.
- [7] A. Verma, A. Jain, A. Tiwari, S. Saraf, P.K. Panda, G.P. Agrawal, S.K. Jain, Folate conjugated double liposomes bearing prednisolone and methotrexate for targeting rheumatoid arthritis, *Pharm. Res. (N. Y.)* 36 (2019) 123, <https://doi.org/10.1007/s11095-019-2653-0>.
- [8] C. Sacchetti, R. Liu-Bryan, A. Magrini, N. Rosato, N. Bottini, M. Bottini, Polyethylene-glycol-modified single-walled carbon nanotubes for intra-articular delivery to chondrocytes, *ACS Nano* 8 (2014) 12280–12291, <https://doi.org/10.1021/nn504537b>.
- [9] M. Nakamura, Y. Tahara, Y. Ikehara, T. Murakami, K. Tsuchida, S. Iijima, I. Waga, M. Yudasaka, Single-walled carbon nanohorns as drug carriers: adsorption of prednisolone and anti-inflammatory effects on arthritis, *Nanotechnology* 22 (2011) 465102, <https://doi.org/10.1088/0957-4484/22/46/465102>.
- [10] Y. Zhao, Z. He, R. Wang, P. Cai, X. Zhang, Q. Yuan, J. Zhang, F. Gao, X. Gao, Comparison of the therapeutic effects of gold nanoclusters and gold nanoparticles on rheumatoid arthritis, *J. Biomed. Nanotechnol.* 15 (2019) 2281–2290, <https://doi.org/10.1166/jbn.2019.2848>.
- [11] H.J. Kim, S.M. Lee, K.H. Park, C.H. Mun, Y.B. Park, K.H. Yoo, Drug-loaded gold/iron/gold plasmonic nanoparticles for magnetic targeted chemo-photothermal treatment of rheumatoid arthritis, *Biomaterials* 61 (2015) 95–102, <https://doi.org/10.1016/j.biomaterials.2015.05.018>.
- [12] N. Yin, X. Tan, H. Liu, F. He, N. Ding, J. Gou, T. Yin, H. He, Y. Zhang, X. Tang, A novel indomethacin/methotrexate/MMP-9 siRNA *in situ* hydrogel with dual effects of anti-inflammatory activity and reversal of cartilage disruption for the synergistic treatment of rheumatoid arthritis, *Nanoscale* 12 (2020) 8546–8562, <https://doi.org/10.1039/d0nr00454e>.
- [13] J. Seo, S.H. Park, M.J. Kim, H.J. Ju, X.Y. Yin, B.H. Min, M.S. Kim, Injectable Click-Crosslinked hyaluronic acid depot to prolong therapeutic activity in articular joints affected by rheumatoid arthritis, *ACS Appl. Mater. Interfaces* 11 (2019) 24984–24998, <https://doi.org/10.1021/acsami.9b04979>.

- [14] H. Wang, Z. Yang, Short-peptide-based molecular hydrogels: novel gelation strategies and applications for tissue engineering and drug delivery, *Nanoscale* 4 (2012) 5259–5267, <https://doi.org/10.1039/c2nr31149f>.
- [15] W. Ma, S.N. Sha, P.L. Chen, M. Yu, J.J. Chen, C.B. Huang, B. Yu, Y. Liu, L.H. Liu, Z.Q. Yu, A cell Membrane-Targeting Self-Delivery chimeric peptide for enhanced photodynamic therapy and in situ therapeutic feedback, *Adv. Healthc. Mater.* 9 (2020), e1901100, <https://doi.org/10.1002/adhm.201901100>.
- [16] Y. Zhong, J. Zhan, G. Xu, Y. Chen, Q. Qin, X. Liao, S. Ma, Z. Yang, Y. Cai, Enzyme-Instructed Self-Assembly enabled Monomer-Excimer transition to construct higher ordered luminescent supramolecular assembly for activity-based bioimaging, *Angew Chem. Int. Ed. Engl.* 60 (2021) 8121–8129, <https://doi.org/10.1002/anie.202014278>.
- [17] Y. Cai, H. Shen, J. Zhan, M. Lin, L. Dai, C. Ren, Y. Shi, J. Liu, J. Gao, Z. Yang, Supramolecular "trojan horse" for nuclear delivery of dual anticancer drugs, *J. Am. Chem. Soc.* 139 (2017) 2876–2879, <https://doi.org/10.1021/jacs.6b12322>.
- [18] J. Nam, H.K. Lim, N.H. Kim, J.K. Park, E.S. Kang, Y.T. Kim, C. Heo, O.S. Lee, S.G. Kim, W.S. Yun, M. Suh, Y.H. Kim, Supramolecular peptide Hydrogel-Based soft neural interface augments brain signals through a Three-Dimensional electrical network, *ACS Nano* 14 (2020) 664–675, <https://doi.org/10.1021/acsnano.9b07396>.
- [19] M.J. Webber, J. Tongers, C.J. Newcomb, K.T. Marquardt, J. Bauersachs, D.W. Losordo, S.I. Stupp, Supramolecular nanostructures that mimic VEGF as a strategy for ischemic tissue repair, *Proc. Natl. Acad. Sci. U. S. A.* 108 (2011) 13438–13443, <https://doi.org/10.1073/pnas.1016546108>.
- [20] B. Senturk, B.M. Demircan, A.D. Ozkan, S. Tohumeken, T. Delibasi, M.O. Guler, A.B. Tekinay, Diabetic wound regeneration using heparin-mimetic peptide amphiphile gel in db/db mice, *Biomater. Sci.* 5 (2017) 1293–1303, <https://doi.org/10.1039/c7bm00251c>.
- [21] C. Yang, L. Chu, Y. Zhang, Y. Shi, J. Liu, Q. Liu, S. Fan, Z. Yang, D. Ding, D. Kong, J. Liu, Dynamic biostability, biodistribution, and toxicity of L/D-peptide-based supramolecular nanofibers, *ACS Appl. Mater. Interfaces* 7 (2015) 2735–2744, <https://doi.org/10.1021/am507800e>.
- [22] J. Liu, J. Liu, L. Chu, Y. Zhang, H. Xu, D. Kong, Z. Yang, C. Yang, D. Ding, Self-assembling peptide of D-amino acids boosts selectivity and antitumor efficacy of 10-hydroxycamptothecin, *ACS Appl. Mater. Interfaces* 6 (2014) 5558–5565, <https://doi.org/10.1021/am406007g>.
- [23] J. Li, Y. Kuang, Y. Gao, X. Du, J. Shi, B. Xu, D-amino acids boost the selectivity and confer supramolecular hydrogels of a nonsteroidal anti-inflammatory drug (NSAID), *J. Am. Chem. Soc.* 135 (2013) 542–545, <https://doi.org/10.1021/ja310019x>.
- [24] J. Zhou, X. Du, N. Yamagata, B. Xu, Enzyme-Instructed Self-Assembly of small D-Peptides as a Multiple-Step process for selectively killing cancer cells, *J. Am. Chem. Soc.* 138 (2016) 3813–3823, <https://doi.org/10.1021/jacs.5b13541>.
- [25] D. Aletaha, J.S. Smolen, Diagnosis and management of rheumatoid arthritis: a review, *JAMA* 320 (2018) 1360–1372, <https://doi.org/10.1001/jama.2018.13103>.
- [26] Z. Wen, J. Zhan, H. Li, G. Xu, S. Ma, J. Zhang, Z. Li, C. Ou, Z. Yang, Y. Cai, M. Chen, Dual-ligand supramolecular nanofibers inspired by the renin-angiotensin system for the targeting and synergistic therapy of myocardial infarction, *Theranostics* 11 (2021) 3725–3741, <https://doi.org/10.7150/thno.53644>.
- [27] W. Guo, W. Feng, J. Huang, J. Zhang, X. Fan, S. Ma, M. Li, J. Zhan, Y. Cai, M. Chen, Supramolecular Self-Assembled nanofibers efficiently activate the precursor of hepatocyte growth factor for angiogenesis in myocardial infarction therapy, *ACS Appl. Mater. Interfaces* 13 (2021) 22131–22141, <https://doi.org/10.1021/acsnano.0c23153>.
- [28] C. Yang, L. Chu, Y. Zhang, Y. Shi, J. Liu, Q. Liu, S. Fan, Z. Yang, D. Ding, D. Kong, J. Liu, Dynamic biostability, biodistribution, and toxicity of L/D-peptide-based supramolecular nanofibers, *ACS Appl. Mater. Interfaces* 7 (2015) 2735–2744, <https://doi.org/10.1021/am507800e>.
- [29] Z. Wu, M. Tan, X. Chen, Z. Yang, L. Wang, Molecular hydrogelators of peptoid-peptide conjugates with superior stability against enzyme digestion, *Nanoscale* 4 (2012) 3644–3646, <https://doi.org/10.1039/c2nr30408b>.
- [30] Y. Lu, L. Li, Y. Zhu, X. Wang, M. Li, Z. Lin, X. Hu, Y. Zhang, Q. Yin, H. Xia, C. Mao, Multifunctional Copper-Containing carboxymethyl Chitosan/Alginate scaffolds for eradicating clinical bacterial infection and promoting bone formation, *ACS Appl. Mater. Interfaces* 10 (2018) 127–138, <https://doi.org/10.1021/acsami.7b13750>.
- [31] A.B. Nair, S. Jacob, A simple practice guide for dose conversion between animals and human, *J. Basic Clin. Pharm.* 7 (2016) 27–31, <https://doi.org/10.4103/0976-0105.177703>.
- [32] Y. Lu, L. Li, Z. Lin, L. Wang, L. Lin, M. Li, Y. Zhang, Q. Yin, Q. Li, H. Xia, A new treatment modality for rheumatoid arthritis: combined photothermal and photodynamic therapy using Cu_(7.2)S₍₄₎ nanoparticles, *Adv. Healthc. Mater.* 7 (2018), e1800013, <https://doi.org/10.1002/adhm.201800013>.
- [33] C. Ren, Y. Gao, J. Liu, Y. Zhang, G. Pu, L. Yang, F. Huang, C. Yang, Z. Yang, J. Liu, Anticancer supramolecular hydrogel of D/L-Peptide with enhanced stability and bioactivity, *J. Biomed. Nanotechnol.* 14 (2018) 1125–1134, <https://doi.org/10.1166/jbn.2018.2564>.
- [34] E. Neumann, S. Lefevre, B. Zimmermann, S. Gay, U. Müller-Ladner, Rheumatoid arthritis progression mediated by activated synovial fibroblasts, *Trends Mol. Med.* 16 (2010) 458–468, <https://doi.org/10.1016/j.molmed.2010.07.004>.
- [35] M. Cutolo, A. Sulli, C. Pizzorni, B. Serio, R.H. Straub, Anti-inflammatory mechanisms of methotrexate in rheumatoid arthritis, *Ann. Rheum. Dis.* 60 (2001) 729–735, <https://doi.org/10.1136/ard.60.8.729>.
- [36] Y. Bedoui, X. Guillot, J. Sélambarom, P. Guiraud, C. Giry, M.C. Jaffar-Bandjee, S. Ralandison, P. Gasque, Methotrexate an old drug with new tricks, *Int. J. Mol. Sci.* 20 (2019) 5023, <https://doi.org/10.3390/ijms20205023>.
- [37] M.A. Boutet, G. Courties, A. Nerviani, B. Le Goff, F. Apparailly, C. Pitzalis, F. Blanchard, Novel insights into macrophage diversity in rheumatoid arthritis synovium, *Autoimmun. Rev.* 20 (2021) 102758, <https://doi.org/10.1016/j.autrev.2021.102758>.
- [38] J. Li, H.C. Hsu, J.D. Mountz, Managing macrophages in rheumatoid arthritis by reform or removal, *Curr. Rheumatol. Rep.* 14 (2012) 445–454, <https://doi.org/10.1007/s11926-012-0272-4>.
- [39] I.A. Udalova, A. Mantovani, M. Feldmann, Macrophage heterogeneity in the context of rheumatoid arthritis, *Nat. Rev. Rheumatol.* 12 (2016) 472–485, <https://doi.org/10.1038/nrrheum.2016.91>.
- [40] F. Hao, R.J. Lee, L. Zhong, S. Dong, C. Yang, L. Teng, Q. Meng, J. Lu, J. Xie, L. Teng, Hybrid micelles containing methotrexate-conjugated polymer and co-loaded with microRNA-124 for rheumatoid arthritis therapy, *Theranostics* 9 (2019) 5282–5297, <https://doi.org/10.7150/thno.32268>.
- [41] L. Zhang, J. Chang, Y. Zhao, H. Xu, T. Wang, Q. Li, L. Xing, J. Huang, Y. Wang, Q. Liang, Fabrication of a triptolide-loaded and poly-γ-glutamic acid-based amphiphilic nanoparticle for the treatment of rheumatoid arthritis, *Int. J. Nanomed.* 13 (2018) 2051–2064, <https://doi.org/10.2147/IJN.S151233>.
- [42] W. Qi, C. Lin, K. Fan, Z. Chen, L. Liu, X. Feng, H. Zhang, Y. Shao, H. Fang, C. Zhao, R. Zhang, D. Cai, Hesperidin inhibits synovial cell inflammation and macrophage polarization through suppression of the PI3K/AKT pathway in complete Freund's adjuvant-induced arthritis in mice, *Chem. Biol. Interact.* 306 (2019) 19–28, <https://doi.org/10.1016/j.cbi.2019.04.002>.
- [43] Q. Guo, Y. Wang, D. Xu, J. Nossent, N.J. Pavlos, J. Xu, Rheumatoid arthritis: pathological mechanisms and modern pharmacologic therapies, *Bone Res* 6 (2018) 15, <https://doi.org/10.1038/s41413-018-0016-9>.